Astronomy & Astrophysics manuscript no. wtheta˙v9
November 5, 2013
© ESO 2013

Herschel ATLAS:⋆ The angular correlation function of submillimetre galaxies at high and low redshift.

S.J. Maddox[1], L. Dunne[1], E. Rigby[1], S. Eales[2], A. Cooray[9], D. Scott[18], J.A. Peacock[19], M. Negrello[16], D.J.B. Smith[1], D. Benford[15], A. Amblard[9], R. Auld[2], M. Baes[3], D. Bonfield[4], D. Burgarella[5], S. Buttiglione[6], A. Cava[7,20], D. Clements[8], A. Dariush[2], G. de Zotti[6], S. Dye[2], D. Frayer[10], J. Fritz[3], J. Gonzalez-Nuevo[11], D. Herranz[12], E. Ibar[13], R. Ivison[13], M.J. Jarvis[4], G. Lagache[14], L. Leeuw[15], M. Lopez-Caniego[12], E. Pascale[2], M. Pohlen[2], G. Rodighiero[6], S. Samui[11], S. Serjeant[16], P. Temi[15], M. Thompson[4], and A. Verma[17]

(Affiliations can be found after the references)

arXiv:1005.2406v1 [astro-ph.CO] 13 May 2010

ABSTRACT

We present measurements of the angular correlation function of galaxies selected from the first field of the H-ATLAS survey. Careful removal of the background from galactic cirrus is essential, and currently dominates the uncertainty in our measurements. For our 250 μm-selected sample we detect no significant clustering, consistent with the expectation that the 250 μm-selected sources are mostly normal galaxies at $z \lesssim 1$. For our 350 μm and 500 μm-selected samples we detect relatively strong clustering with correlation amplitudes A of 0.2 and 1.2 at $1'$, but with relatively large uncertainties. For samples which preferentially select high redshift galaxies at $z \sim 2-3$ we detect significant strong clustering, leading to an estimate of $r_0 \sim 7-11\,h^{-1}$ Mpc. The slope of our clustering measurements is very steep, $\delta \sim 2$. The measurements are consistent with the idea that sub-mm sources consist of a low redshift population of normal galaxies and a high redshift population of highly clustered star-bursting galaxies.

Key words. Submm galaxies –Galaxy clustering

1. Introduction

Submillimetre (sub-mm) selected galaxy samples provide a unique way to trace obscured star formation out to high redshifts (Blain et al. 2002). Models for the evolution of such populations disagree on the nature of the sub-mm sources at high redshifts, with some claiming that they are massive galaxies in the process of forming most of their stellar mass (Granato et al. 2004, Narayanan et al. 2009, Davé et al. 2010) while others model them as lower mass sources undergoing bursts of star formation with a top heavy IMF (Baugh et al. 2005, Lacey et al. 2009). While evidence on individual sources largely supports a massive halo scenario (Dunne, Eales & Edmunds 2003, Swinbank et al. 2008, Michalowski, Hjorth & Watson 2010), the best way to measure the statistical halo properties of this population is to measure their clustering. The three-dimensional clustering of sub-mm galaxies provides information about the dark-matter halos that they populate, but direct measurements need distance estimates for each galaxy, which we do not have for our sample. The angular clustering can be measured for flux-limited samples but, in order to compare with models, predictions are required for both the $n(z)$ of flux limited samples and the intrinsic 3-d clustering of the galaxies. The sub-mm colours depend on the source redshift, and so selecting on colour can preferentially select high or low redshift samples (see e.g. Amblard et al. 2010).

Previous attempts to measure the clustering of sub-mm sources have been mostly based on catalogues which cover only very small areas. Despite predictions that sub-mm galaxies should have high spatial clustering, their $n(z)$ is broad and so previous work has had limited success in detecting a significant angular clustering signal (Blain et al. 2004, Scott et al. 2006, Weiß et al. 2010). A more recent approach has been to measure the power spectrum of larger area sub-mm maps from BLAST (Viero et al. 2009, Devlin et al. 2009). This analysis has found significant evidence for clustering, although at relatively low amplitude.

The *Herschel* ATLAS (H-ATLAS) (Eales et al. 2010) will survey over 550 deg^2 in 5 wavebands at 100, 160, 250, 350 and 500 μm. One field covering $\sim 4^\circ \times 4^\circ$ degrees was observed during the science demonstration phase of the mission, and has produced a catalogue of $\sim$ 6600 sources with significance $> 5\sigma$ above the combined instrumental and confusion noise. This represents roughly 1/30 of the final H-ATLAS data-set. In this paper we present measurements of the angular correlation function of five flux and colour-selected samples of the H-ATLAS sources.

2. H-ATLAS data and source catalogues

H-ATLAS uses parallel scan mode observations performed with the ESA *Herschel* Space Observatory (Pilbratt et al. 2010), providing data simultaneously from both the PACS (Poglitsch et al. 2010) and SPIRE (Griffin et al. 2010) instruments. The time-line data are reduced using HIPE. Maps are produced from the SPIRE data using a naive mapping technique after removing instrumental temperature variations from the time-line data (Pascale et al. in prep). Noise maps are generated by using the two cross-scan measurements to estimate the noise per detector pass, and then for each pixel the noise is scaled by $N_{passes}^{1/2}$, where N_{passes} is the number of detector passes. A false-colour image combining the SPIRE 250, 350 and 500 μm maps is shown in Fig. 1. The PACS H-ATLAS maps currently yield only a few hundred sources, which is insufficient for us to attempt a clustering mea-

⋆ *Herschel* is an ESA space observatory with science instruments provided by European-led Principal Investigator consortia and with important participation from NASA.

Fig. 1. False-colour image combining the SPIRE 250, 350 and 500 μm maps as blue, green and red respectively. The ragged edges show the individual scan-legs of the two scans. Galactic cirrus can be seen as patchy blue wisps over the field.

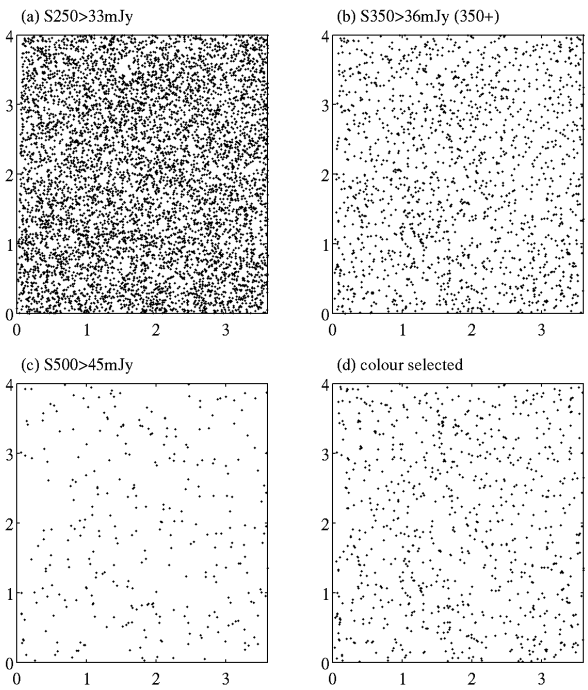

Fig. 2. The positions of sources in four subsamples (a) $S_{250} >$ 33mJy; (b) $S_{350} >$ 36mJy and 3σ in S_{250} and S_{500} (the 350+ sample); (c) $S_{500} >$ 45mJy; (d) the colour selected sample $S_{500}/S_{250} > 0.75$.

surement. The clustering in the PACS bands will be investigated in a future paper using more data.

Sources were identified in the SPIRE maps using a Multi-band Algorithm for source eXtraction (MADX, Maddox et al. in prep). First a local background is estimated from the peak of the histogram of pixel values in 30×30 blocks of pixels. This corresponds to 2.5′ for the 250 μm map, and 5′ for the 350 and 500 μm maps. The background at each pixel is then estimated using a bi-cubic interpolation between the coarse grid of backgrounds, and this value subtracted from the pixel. The filter scale was chosen to be as large as possible while still following the variations in the cirrus background. Since the local background is estimated from the peak of the flux histogram, it is insensitive to the presence of resolved sources within the background block, so long as they do not cover a significant number of pixels in the block. This approach should remove the local background without removing flux from the resolved sources, and so should be less susceptible to removing real structure in the source distribution compared to standard Fourier filtering approaches.

The background subtracted maps are then filtered by the estimated PSF, including a local inverse variance weighting. The maps from all three bands are then combined with weights set by the local inverse variance, and also the prior expectation of the SED of the galaxies. We tried a flat-spectrum prior, where equal weight is given to each band and also 250 μm weighting, where only the 250 μm band was included. At the depth of the filtered maps source confusion becomes an issue in the longer wavelength bands, and the higher resolution of the 250 μm maps outweighs the signal-to-noise gain from adding in the other bands. The current catalogues use the 250 μm-only prior and we will revisit this issue in future data releases.

All local peaks are identified in the combined PSF filtered map as potential sources, and a Gaussian is fitted to each peak to give estimates of the position at the sub-pixel level and the point source flux. The flux densities in other bands are estimated by using a bi-cubic interpolation to the position given by the combined map. To produce a catalogue of reliable sources, we select only sources that are detected at the 5-σ level in any of the bands. In calculating the σ for each source, we use the relevant noise map, and add the confusion noise to this in quadrature. The average 1-σ instrumental noise values in the PSF-filtered maps are 4, 4 and 5.7mJy beam^{-1} respectively in the 250, 350 and 500 μm bands. We estimated the confusion noise from the difference between the variance of the maps and the expected variance due to instrumental noise, and find that the 1-σ confusion noise is 5, 6 and 7 mJy beam^{-1} at 250, 350 and 500 μm. The resulting total 5-σ limits are 33, 36 and 45mJy beam^{-1} (Rigby et al. in prep). Source counts from these catalogues are analysed by Clements et al. (2010), and are found to be consistent with previous measurements in these wave-bands (Patanchon et al. 2009).

We have selected five samples to use for our current clustering analysis. The first three use simple flux density cuts, as given in Table 1. The fourth and fifth samples are as defined by Amblard et al. (2010), who use the H-ATLAS colours to estimate redshift distributions. The fourth sample, which we call 350+ is $> 5\sigma$ at 350μm with an extra constraint that the sources must also be detected at more than 3σ in the 250 μm and 500 μm bands, and the fifth sample adds a further constraint that the ratio $S_{500}/S_{250} > 0.75$. Requiring a detection at 500 μm tends to select higher redshift galaxies compared to a simple 350 μm selection, and Amblard et al. estimate that the mean redshift of the 350+ sample is 2.2 ± 0.6. The $S_{500}/S_{250} > 0.75$ colour selection pushes to an even higher redshift, of 2.6 ± 0.3. The positions of sources in four of the sub-samples are shown in Fig. 2.

3. Measuring $w(\theta)$

We measure the correlation function by counting pairs in the data as a function of angular separation and comparing to the number of pairs in a random catalogue with similar boundaries and selection effects. The pair counts are combined to estimate the

Table 1. Subsamples used to measure $w(\theta)$, and best-fit power-law parameters. N is the number of sources in each sample. A is the amplitude at $1'$ and δ is the power-law slope. $A_{0.8}$ and $A_{2.0}$ are the amplitudes at $1'$ with the slopes fixed at 0.8 and 2.0 respectively.

Sample	N	A	δ	$A_{0.8}$	$A_{2.0}$
$S_{250} > 33$	6317	-0.01 ± 0.07	1.7 ± 0.2	-0.00	-0.01
$S_{350} > 36$	2754	0.20 ± 0.07	2.0 ± 0.2	0.11	0.20
$S_{350} > 36^*$	1633	0.50 ± 0.09	2.8 ± 0.5	0.21	0.50
$S_{500} > 45$	304	1.24 ± 1.6	2.4 ± 1.3	0.51	1.24
$S_{500}/S_{250} > 0.75$	808	0.92 ± 0.3	2.1 ± 0.5	0.38	0.92

* this is the 350+ sample which has the additional constraint that source must be detected at $> 3\sigma$ in the other two bands.

correlation function, $w(\theta)$, using the Landy & Szalay estimator (1993)

$$w(\theta) = \frac{DD - 2DR + RR}{RR}. \quad (1)$$

Here DD is the number of data-data pairs, DR is the number of data-random pairs and RR is the number of random-random pairs, each at separation θ.

The random catalogues were generated to follow the sensitivity limit of the actual data selection. This means that any non-uniformities in the data due to variation in signal-to-noise should not be imprinted on the clustering signal. To relate the noise at a pixel to the expected number density of sources we generated random fluxes which match the observed count slope (Clements et al. 2010), perturbed them by a Gaussian deviate with standard deviation equal to the local noise estimate, and then kept the random source if it was brighter than the chosen flux limit. In practice the noise maps are uniform enough that using uniform random catalogues makes no significant difference to the results.

The clustering measurements are sensitive to the correct removal of the spatially varying cirrus background, as well as the unresolved background of faint sources, which are also likely to be strongly clustered. We have investigated the stability of the measurements by masking areas around the brightest patches of cirrus. This had little effect on the measurements indicating that our cirrus removal is effective. Increasing the scale of background filtering to 60 and 120 pixels produces a much larger clustering signal. A visual inspection of the source positions makes it clear that the excess structure in the source distribution is correlated with the pattern of cirrus emission, and so is likely to be spurious signal caused by insufficient background subtraction.

A potential concern when using such a small scale to remove the background is that some real clustering may have been removed. This was tested by using clustered source positions to create simulated maps, which include cirrus background estimated from the IRAS maps (Schlegel Finkbeiner & Davis 1998) and the same noise and coverage maps as the real data. The background was then filtered and sources extracted using the MADX algorithm as for the real data, and the clustering of the resulting sources measured. The clustering amplitude recovered from the simulations varied with background subtraction scale in a similar way to the real data. The correct amplitude was recovered using 30 pixels; using 15 pixels underestimated the amplitude by $\sim 10\%$. We therefore believe that our background subtraction has removed the effect of cirrus on the source clustering, yet has not removed true structure in the source distribution.

Our measurements of $w(\theta)$ are shown in Fig. 3. The panels (a) and (c) show the flux limited samples in the 250 and 500 μm, bands while panel (b) shows the 350+ sample and panel (d) the $S_{500}/S_{250} > 0.75$ colour selected sample. The error bars on the plots are estimated from the Poisson noise in the pair counts. We fitted the data using a simple power law of the form $w(\theta) = A\theta^{-\delta}$, corrected for the integral constraint using the Roche and Eales (1999) technique. The power law slopes, δ and amplitudes at 1 arc minute, A are given in Table1. Uncertainties on these measurements were estimated by fitting power laws to Monte-Carlo realizations of the data, and measuring the standard deviation of the resulting parameters.

4. Discussion

The S_{250} sample has no detectable clustering signal. The simple S_{350} flux limited sample does show fairly significant clustering at scales $\lesssim 2'$, but the 350+ sample produces a higher amplitude and more significant detection, as expected given that adding cuts in the other two bands leads to a narrower $n(z)$ by removing low-z galaxies. The S_{500} sample gives a noisier $w(\theta)$, but also shows a high amplitude. The colour-selected sample with $S_{500}/S_{250} > 0.75$ shows a higher amplitude, and higher noise compared to the 350+ sample. The power-law fits to all samples give steep slopes $\delta \sim 2$.

The increasing amplitude in samples selected at longer wavelengths suggests that clustering is stronger in the higher redshift populations, since selection at longer wavelengths tends to favour higher redshift galaxies. According to some models, these are highly clustered star-burst galaxies which are the ancestors of present day ellipticals (Negrello et al. 2007, Davé et al. 2010). The two samples with additional color cuts have $n(z)$ from photometric redshifts derived by Amblard et al. 2010. which can be used to convert the angular amplitudes to spatial r_0. For both samples we find a range of $r_0 \sim 7-11h^{-1}$ Mpc, depending on the slope used ($\delta = 2$ or $\delta = 0.8$ respectively). While the slope we measure at scales of a few arcmin is universally steep we cannot be sure with the current data-set what the behaviour will be at larger scales. A larger data set is required to fully address the behaviour of the slope and hence reduce the uncertaintites in r_0.

At first sight, the non-detection of clustering in the 250 μm sample is somewhat surprising. It contains a high fraction of lower redshift galaxies, with > 30 percent at $z < 1$ (Smith et al. in prep). This low-z population is expected to cluster in a similar way to local optical galaxies. Galaxies in the SDSS with magnitudes $21 < r^* < 22$ have a correlation amplitude of 0.046 at $1'$ (Connolly et al. 2002). Also most of the 350 μm sample is a subset of the 250 μm sample, so their clustering will contribute to the 250 μm clustering. Assuming they are uncorrelated with the low-z galaxies, they will contribute an amplitude scaled down by the relative density squared, leading to an expected amplitude ~ 0.03. These relatively small amplitudes are consistent with our measurement of -0.01 ± 0.07.

Overall, these results are consistent with the general expectation from models which include highly clustered high redshift and weakly clustered low redshift populations of sub-mm emitting galaxies. Models which postulate that sub-mm sources have a higher mass IMF than normal (Baugh et al. 2005, Lacey et al. 2010) predict a higher clustering strength at lower redshifts, which seems at first glance to be at odds with our result. However, these models do predict far stronger clustering above a threshold in luminosity which is redshift dependent. It is possible that our high-z samples exceed this threshold while the low-z

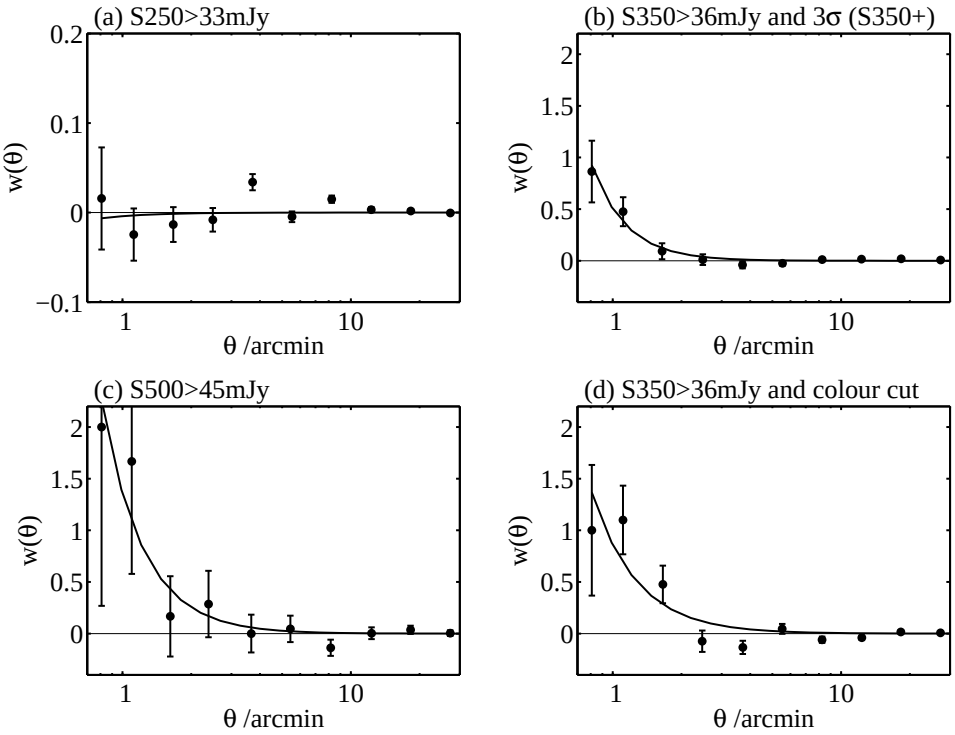

Fig. 3. Plot of $w(\theta)$ for four subsamples discussed in the text. The panels show (a) $S_{250} > 33$mJy, (b) $S_{350} > 36$mJy with 3σ detections in the 250 μm and 500 μm bands (the 350+ sample), (c) $S_{500} > 45$mJy, and (d) $S_{350} > 36$mJy with 3σ and $S_{500}/S_{250} > 0.75$ colour selected sample. The error bars on the plots are estimated from the Poisson noise in the pair counts. Note the expanded scale on panel (a).

samples do not. It is beyond the scope of the current data set to be able to confirm or rule out these models.

There are few previous observations to compare to directly, and those that are available have rather different selections and redshift distributions. Magliocchetti et al. (2008) analysed the distribution of bright 24 μm sources with faint optical counterparts, split into high ($\langle z \rangle \sim 2$) and low redshift ($\langle z \rangle \sim 0.8$) subsamples. They found a low amplitude ($A \sim 0.14 \pm 0.05$) at low redshift and a higher amplitude ($A \sim 0.26 \pm 0.1$) at high redshift. This trend of $w(\theta)$ increasing towards higher z is similar to our observations.

The power spectrum analysis of the BLAST data by Viero et al. (2009) detects clustering on scales $5' < \theta < 20'$. Once interpreted within the Halo Model formalism, their measurement points to an increase in the spatial clustering of the background sub-mm source population with increasing wavelength and therefore increasing redshift. Again this is consistent with our findings.

LABOCA observations of the extended Chandra Deep Field South have produced a catalogue of 126 sources selected at 850 μm (Weiß et al 2009). A weak detection of clustering is found on scales $\theta < 2'$. Fixing the slope to be 0.8, their power-law fit has an amplitude of 0.18 ± 0.1 at $1'$. This is similar to the amplitude that we find for the 350 μm selected sample.

Though all three of these measurements are similar to ours, it is not simple to make a direct comparison because either or both of the flux-limit or pass-bands are different, and so the redshift distributions are not the same.

Given the statistical limitations on the current small field, we leave detailed comparisons to models to a later analysis with more data. However we can say that our measurements appear to be consistent with the prevailing models, where sub-mm sources consist of a low redshift population of normal star-forming disk galaxies that have a spatial correlation length, $r_0 \sim 4$ Mpc, and a high redshift population of highly clustered star-bursting galaxies $r_0 \sim 10$Mpc (Negrello et al. 2007, Narayanan et al. 2009, Davé et al. 2010). The rather steep slope of our measurements for the higher redshift samples is also consistent with the high redshift population forming in compact protoclusters.

The current field is only 1/30 of the area that H-ATLAS will cover, and it has the brightest cirrus background of the planned fields. The final H-ATLAS dataset will have much larger fields with lower cirrus emission, and so will provide a benchmark measurement of source clustering in sub-mm populations.

References

Amblard, A et al., 2010 A&A, this volume
Baugh et al., 2005, MNRAS, 356, 1191
Blain, A.W., Smail, I., Ivison, R.J., Kneib, J-P., & Frayer, D., 2002, Phys. Rep., 369, 111.
Blain, A.W., Chapman, S.C., Smail, I., Ivison, R., 2004, ApJ, 611, 725
Clements D., et al., A&A this volume.
Connolly, A., et al., 2002, Ap J, 579, 42.
Davé, R., Finlator, K., Oppenheimer, B.D., Fardal, M., Katz, N., Kereš, D., Weinberg, D.H., 2010, MNRAS, 404, 1355.
Devlin, M.J., et al., 2009, Nature 458, 737.
Dunne, L., Eales, S., Edmunds, M.G., 2003, MNRAS, 341, 589.
Eales, S., et al., PASP, 122, 499.
Granato G.L., De Zotti G., Silva L., Bressan A., Danese L., 2004, ApJ, 600, 580
Griffin, M., et al. 2010 A&A this volume.
Landy, S.D., and Szalay, A.S, 1993, Ap J, 412, 64
Lacey, C.G., et al., 2009, arXiv0909.1567
Magliocchetti, M., et al., 2008 MNRAS, 383 1131

Michalowski, M., Hjorth, J., & Watson, D., 2010, A&A, in press, arXiv0905.4499M
Narayanan, D., et al., 2009, MNRAS, submitted, 2009arXiv0910.2234N
Negrello, M., et al., 2007 MNRAS, 377, 1557
Patanchon, G., et al. 2009 ApJ, 707, 1750
Pilbratt, G., et al. A&A this volume.
Poglitsch, A., et al. 2010 A&A this volume.
Roche, N., & Eales, S., 1999, MNRAS, 307, 703
Schlegel, D., Finkbeiner, D., Davis, M., 1998, ApJ, 500, 525.
Scott, S.E., Dunlop, J. S., Serjeant, S., 2006, MNRAS, 370, 1057
Swinbank, M., et al. 2008 MNRAS, 391, 420
Weiß, A., et al. 2009, ApJ 707, 1201.
Viero, M.P., et al., 2009 ApJ 707, 1766.

---

[1] School of Physics and Astronomy, University of Nottingham, University Park, Nottingham NG7 2RD, UK
[2] School of Physics and Astronomy, Cardiff University, The Parade, Cardiff, CF24 3AA, UK
[3] Sterrenkundig Observatorium, Universiteit Gent, Krijgslaan 281 S9, B-9000 Gent, Belgium
[4] Centre for Astrophysics Research, Science and Technology Research Centre, University of Hertfordshire, Herts AL10 9AB, UK
[5] Laboratoire d'Astrophysique de Marseille, UMR6110 CNRS, 38 rue F. Joliot-Curie, F-13388 Marseille France
[6] University of Padova, Department of Astronomy, Vicolo Osservatorio 3, I-35122 Padova, Italy
[7] Instituto de Astrofísica de Canarias, C/Vía Láctea s/n, E-38200 La Laguna, Spain
[8] Astrophysics Group, Imperial College, Blackett Laboratory, Prince Consort Road, London SW7 2AZ, UK
[9] Dept. of Physics & Astronomy, University of California, Irvine, CA 92697, USA
[10] Infrared Processing and Analysis Center, California Institute of Technology, 770 South Wilson Av, Pasadena, CA 91125, USA
[11] Scuola Internazionale Superiore di Studi Avanzati, via Beirut 2-4, 34151 Triest, Italy
[12] Instituto de Física de Cantabria (CSIC-UC), Santander, 39005, Spain
[13] UK Astronomy Technology Center, Royal Observatory Edinburgh, Edinburgh, EH9 3HJ, UK
[14] Institut d'Astrophysique Spatiale (IAS), B¢timent 121, F-91405 Orsay, France; and Universit Paris-Sud 11 and CNRS (UMR 8617), France
[15] Astrophysics Branch, NASA Ames Research Center, Mail Stop 245-6, Moffett Field, CA 94035, USA
[16] Dept. of Physics and Astronomy, The Open University, Milton Keynes, MK7 6AA, UK
[17] Oxford Astrophysics, Denys Wilkinson Building, University of Oxford, Keble Road, Oxford, OX1 3RH
[18] University of British Colombia, 6224 Agricultural Road, Vancouver, BC V6T 1Z1, Canada
[19] SUPA, Institute for Astronomy, University of Edinburgh, Royal Observatory Edinburgh, Edinburgh, EH9 3HJ, UK
[20] Departamento de Astrofísica, Universidad de La Laguna (ULL), E-38205 La Laguna, Tenerife, Spain